Cation Dependent Surface Charge Regulation in Gated Nanofluidic Devices

Supporting Information

*Marie Fuest, Kaushik K. Rangharajan, Caitlin Boone, A.T. Conlisk, and Shaurya Prakash**

Department of Mechanical and Aerospace Engineering, The Ohio State University, Columbus, OH 43210 USA.

* Corresponding author e-mail: prakash.31@osu.edu

ABSTRACT: The supporting information includes additional data for the experimental observations and models reported in the main manuscript. Specifically, information pertaining to the gate leakage current, concentrations for the electrolyte mixtures, methods used in the numerical COMSOL model to examine the effect of possible inhomogeneous surface charge density of the nanochannel walls as well as pH dependence of nanochannel conductance and surface charge density, and calculation of the interaction parameter for ion-ion correlations are reported.

ELECTRICAL CHARACTERIZATION OF GATED NANOFLUIDIC DEVICE

Applying a potential to the gate electrode modifies the local surface charge density and the local electric field within the nanochannel,[S1-5] which translates to a modulated current. In line with previous reports, the current in the gated case is approximated as the superposition between the axial and gate contributions,[S3,6,7] according to

$$I = G_a V_a + G_g V_g \tag{S1}$$

where, G_a is the intrinsic nanochannel conductance and G_g is the transconductance.[S6,7] The transconductance was determined from linear regression of the measured current I as a function of V_g for fixed axial potentials,[S5] where $V_a = 3V$ and $V_a = 5V$.

Changes in the local dielectric/fluid interface potential induced by the gate electrode modulates the ionic transport and therefore the measured current through the nanochannel.[S3,5] The current was monitored at a broad range of concentrations as the gate voltage (V_g) was swept between +3V and -3V with applied axial potentials (V_a) of 3V and 5V for each experimental condition. Our past report discusses complete device operation with sweeping gate potentials, axial potentials, gate location dependence, and electrolyte concentrations for these nanochannel devices.[S1] A representative plot of measured current for the gate voltage sweep as a function of cation type with $V_a = 3V$ is shown in Figure S1. Four representative cases with the same Debye length, 10 mM KCl, 10 mM NaCl, 3.33 mM $CaCl_2$, and 3.33 mM $MgCl_2$ are shown. The 30 μm wide gate electrode represents a small region compared to the length of the nanochannel. The modulation of nanochannel conductance with a local gate electrode has seen limited investigations[S1,8] and matching known models and experimental observations continues to be a challenge.[S4,9,10]

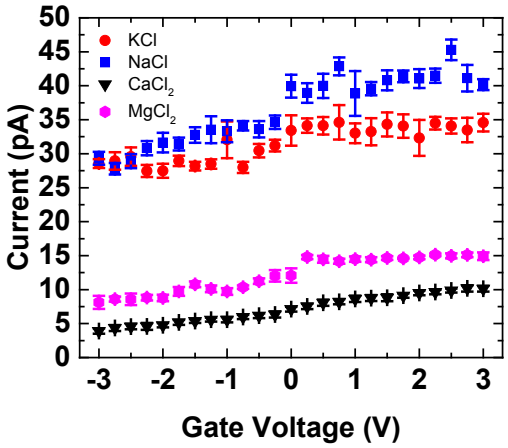

Figure S1. A representative plot of the measured current with the gate voltage sweep as a function of cation type for 10 mM KCl, 10 mM NaCl, 3.33 mM $CaCl_2$, and 3.33 mM $MgCl_2$ with $V_a = 3V$. The ionic strength of the electrolyte solutions was matched to ensure consistent values of the Debye length or the characteristic screening length of the surface potential, across cases. Device operation characteristics and methods have been reported previously.[S1]

GATE LEAKAGE CURRENT

It is often the case in gated nanofluidic devices that the dielectric layer is lossy, permitting a finite gate leakage current.[S1,3,7,11-13] In addition to the axial ion transport current, a finite gate leakage current through the PDMS layer was measured. Leakage current through the PDMS dielectric layer was measured separately for each electrolyte concentration by setting a potential difference between the microchannel reservoir and the gate electrode (grounded) as in previous reports.[S7,13,14] Based on previous reports, a threshold of leakage current/intrinsic current of 1 is set for all measurements,[S1,3] thus limiting the range of gate voltages used in this study to ± 3V. As a representative data set, the bar plots in Figure S2 show the leakage current referenced to intrinsic current for V_a = 3V. In Figure S2, leakage current and ion transport current under gated conditions for 1 mM KCl, 1 mM NaCl, 0.33 mM $CaCl_2$, and 0.33 mM $MgCl_2$ is shown. The ratio shown in the bar plots depends on the leakage current and the ion transport current that contributes to the intrinsic nanochannel conductance.

The intrinsic conductance showed significant cation dependence as discussed in the main manuscript. In order to demonstrate variability of data and the need for multiple measurements over multiple devices with careful experimental controls over electrolyte concentration, pH, and a baseline

intrinsic conductance match for DI water (i.e., 10^{-7} M electrolyte concentration), example data shown here was chosen to provide a broad sample for leakage current values compared to intrinsic current values. The leakage current ratio is higher in the V_a = 3V case (shown below) compared to the V_a = 5V, as expected from the higher intrinsic current with a larger axial potential.

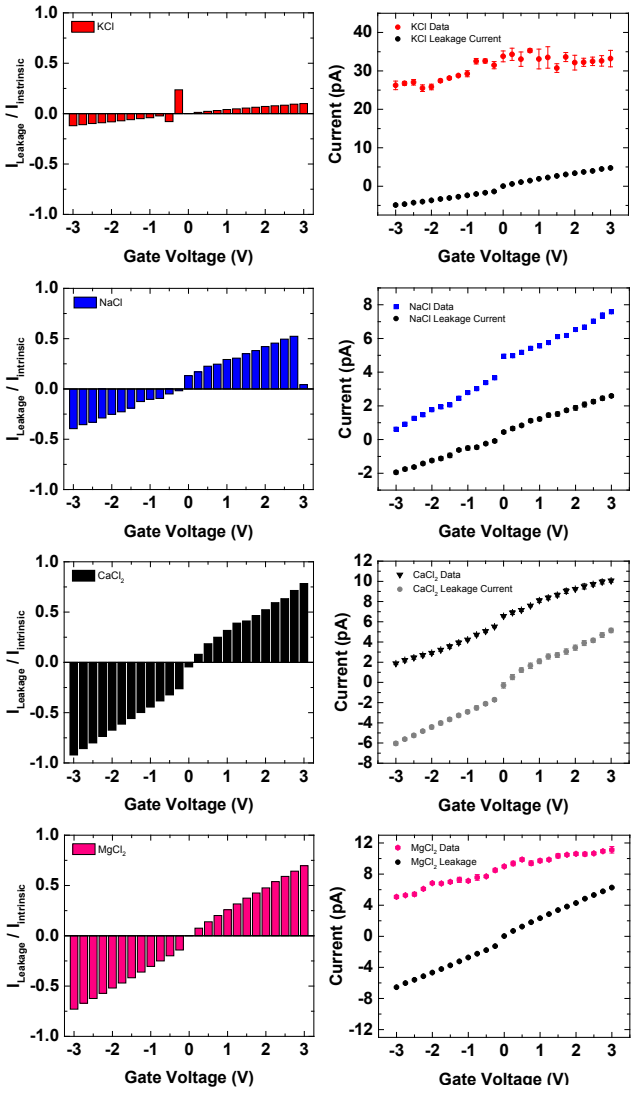

Figure S2. The ratio of the gate leakage current to the intrinsic current (left panels) and the gate leakage current plotted alongside the ion transport current under gated conditions (right panels). The intrinsic conductance varied as a function of cation type, causing variation in the $I_{leakage}/I_{intrinsic}$ across various electrolytes. Example data shown here was selected to provide a range of leakage current values compared to axial current values, highlighting the need for extensive experimental controls that were implemented here and have been discussed throughout the main manuscript and the Supplementary Information. The leakage current ratio is higher in the V_a = 3V case (shown here) compared to the V_a = 5V, as expected from the higher axial transport current with a larger axial potential.

ELECTROLYTE MIXTURES

The following tables summarize the prepared electrolyte compositions (EC) for the electrolyte mixtures used in this work (Table S1), the calculated values of the predicted conductance as a function of electrolyte composition (Table S2), and the measured values of the conductance as a function of electrolyte composition (Table S2). The predicted values (Table S2) were calculated under the assumption of a constant surface charge density across electrolyte composition. As discussed in the main manuscript, the constant surface charge assumption failed to predict the measured intrinsic conductance for the electrolyte mixtures.

Table S1. A summary of electrolyte compositions and the corresponding prepared concentrations.

Electrolyte Composition	Concentrations	Electrolyte Ionic Strength
100% KCl	1 mM KCl	1 mM
75% KCl/25% $CaCl_2$	0.5 mM KCl; 0.17 mM $CaCl_2$	1 mM
50% KCl/50% $CaCl_2$	0.25 mM KCl; 0.25 mM $CaCl_2$	1 mM
25% KCl/75% $CaCl_2$	0.10 mM KCl; 0.30 mM $CaCl_2$	1 mM
100% $CaCl_2$	0.33 mM $CaCl_2$	1 mM

Table S2. Measured and predicted values for the intrinsic conductance as a function of electrolyte composition. Conductance values are given as a ratio of the conductance at a given electrolyte composition over the conductance of the 0% $CaCl_2$ (i.e. 100% KCl case) as discussed in the main manuscript. The conductance values calculated from equations ((S3)-(S6)) below fail to predict the measured conductance indicating the constant surface charge assumption is invalid for electrolyte mixtures.

Electrolyte Composition	$G_{EC}/G_{100\%KCl}$ calculated	$G_{EC}/G_{100\%\ KCl}$ measured
100% KCl	1.00	1.00
75% KCl/25% $CaCl_2$	0.95	0.49
50% KCl/50% $CaCl_2$	0.91	0.42
25% KCl/75% $CaCl_2$	0.89	0.40
100% $CaCl_2$	0.87	0.41

ANALYSIS FOR ELECTROLYTE MIXTURES

The current through the nanochannel is given by equation (S2)

$$I = whF\sum_{i=1}^{m}\mu_i z_i{}^2 c_i{}^{nano} E \tag{S2}$$

where, E is the electric field, z_i is the valence for species i, μ_i is the ionic mobility for species i, and $c_i{}^{nano}$ is the concentration of species i within the nanochannel. Note that equation (1) (main manuscript) is easily derived from equation (S2) by considering that $c_i{}^{nano}$ is determined by the bulk electrolyte concentration and the electroneutrality condition.[S15,16]

The intrinsic nanochannel conductance for an electrolyte mixture prepared from KCl and $CaCl_2$ is then given by

$$G_a = \frac{Fwh}{L}\left(\mu_{K^+}c_{K^+}^{nano} + 4\mu_{Ca^{2+}}c_{Ca^{2+}}^{nano} + \mu_{Cl^-}c_{Cl^-}^{nano}\right) \tag{S3}$$

where c_i^{nano} is the concentration of a species i in the nanochannel and is related to the surface charge density in the surface charge governed regime by $Fhz_ic_i^{nano} = 2\sigma$. Consistent with previous reports for single electrolytes,[S15,17,18] a constant surface charge density was assumed for all electrolyte compositions. Consequently, to maintain system electroneutrality, the space charge within the nanochannel volume must also remain constant across electrolyte compositions (equation (S4)).

Using 0% $CaCl_2$ (or, 100% KCl) as the baseline case, since the space charge is constant the total concentration of all ionic species within the nanochannel is expressed in terms of the concentration of species in the 0% $CaCl_2$ (100% KCl) case as

$$c_{K^+}^{nano} + 2c_{Ca^{2+}}^{nano} + c_{Cl^-}^{nano} = c_{K^+}^{100} \tag{S4}$$

where $c_{K^+}^{100\%}$ is the concentration of K^+ in the nanochannel for the 0% $CaCl_2$ (100% KCl) case.

Consistent with previous work, the relative concentration of cations in the nanochannel is assumed to be equal to the relative concentration of cations in the bulk or reservoir,[S19] that is

$$c_{Ca^{2+}}^{nano} = proCa^{2+} c_{total}^{nano}, \text{ and} \tag{S5}$$

$$c_{K^+}^{nano} = proK^+ c_{total}^{nano} \tag{S6}$$

where $proCa^{2+} = c_{Ca^{2+}}^{bulk}/c_{total}^{bulk}$ and $proK^+ = c_{K^+}^{bulk}/c_{total}^{bulk}$ and $proCa^{2+}$and $proK^+$ are the proportions of Ca^{2+} and K^+ in the bulk solution respectively.

Given that $\mu_{Ca^{2+}} = 0.434\,\mu_{K^+}$,[S20] the conductance at a given electrolyte composition (G_{EC}) can be written in terms of the conductance in the 100% KCl case ($G_{100\%\,KCl}$) from equations ((S3)-(S6)) as

$$\frac{G_{EC}}{G_{100\%\,KCl}} = \left(\frac{1.736proCa^{2+} + proK^+}{2proCa^{2+} + proK^+}\right). \tag{S7}$$

The measured and predicted values of the intrinsic nanochannel conductance as a function of electrolyte composition are shown in Figure 4 of the main manuscript (with values listed in Table S2). The contribution to the conductance from Cl^- ions was neglected since at 1 mM, the electric double layers are strongly interacting[S21] and therefore the nanochannels are expected to be permselective for cations.[S22]

Since the constant surface charge density assumption failed to predict the measured conductance for electrolyte mixtures, the measured conductance was instead used to calculate the value of the effective surface charge density as a function of electrolyte composition. From equations ((S3), (S5), (S6)), and the electroneutrality condition the relative surface charge density at a given electrolyte composition is given by

$$\frac{\sigma_{EC}}{\sigma_0} = \frac{\frac{G_{EC}}{G_{100\%\,KCl}}(2proCa^{2+} + proK^+)}{1.736proCa^{2+} + proK^+} \tag{S8}$$

where σ_{EC} is the surface charge density for a given electrolyte composition and σ_0 is the surface charge density for the 0% $CaCl_2$ (100% KCl) case. The values of $\frac{\sigma_{EC}}{\sigma_0}$ are plotted in Figure 4 of the main manuscript.

NUMERICAL MODEL IN COMSOL MULTIPHYSICS

A 2-D Poisson-Nernst-Planck (PNP) model for ionic transport was implemented using COMSOL Multiphysics. Numerical models were performed for 1 mM KCl and for 0.33 mM $CaCl_2$ as a function of pH. A schematic of the micro- and nanofluidic system modeled using COMSOL is shown in Figure S3.

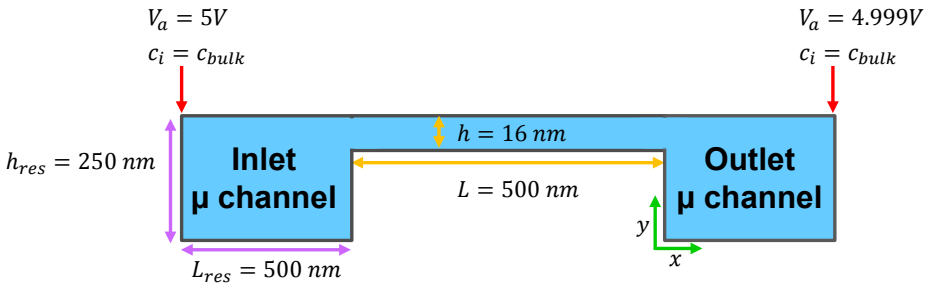

Figure S3: A schematic of the micro- nanofluidic system modeled with COMSOL Multiphysics. Due to the low aspect ratio of the nanochannel (width >> height) the system was modeled in two dimensions.[S20] The inlet and outlet reservoirs, which correspond to the near-infinite reservoirs represented by the microchannels in the fabricated device, were 500 nm long and 250 nm tall. The size of the channel in the model was 16 nm deep x 500 nm long. The concentration in the inlet and outlet reservoirs was set to the bulk electrolyte concentration with all four species considered (that is K^+, Cl^-, OH^-, and H^+ for KCl and Ca^{2+}, Cl^-, OH^-, and H^+ for $CaCl_2$). The axial electric field of 2kV/m was set to match the experimental case V_a = 5V. The location where the concentration and potential boundary conditions were imposed is indicated with the red arrow in the schematic. The surface charge density for each pH was imposed on all surfaces marked with the dark grey line (reservoirs and nanochannel). The magnitude of the surface charge density was the fit parameter used to match the experimentally measured and numerically calculated values of the intrinsic conductance as discussed below.

Due to the use of ultra-low aspect ratio (ULAR) nanochannels (width >> height) considered here the system was modeled in two dimensions.[S20] The size of the channel in the model was 16 nm deep x 500 nm long. The current was calculated according to

$$I = \frac{z_i w F}{L} \int_0^L \int_0^h \sum_i^{m=4} \overrightarrow{N_i} dy dx \qquad \text{(S9)}$$

where, I is the current, z_i is the valence of species i, w is the channel width, F is Faraday's constant, L is the channel length, h is the channel height, and N_i is the flux of the four charged species in the channel. The current calculated with the COMSOL model was multiplied by the number of nanofluidic channels in the fabricated device. Here, the total flux of ions (K^+, Cl^-, OH^-, and H^+ for KCl and Ca^{2+}, Cl^-, OH^-, and H^+

for $CaCl_2$) was integrated across all cross sections along the nanochannel length and then divided by the total length of the channel to obtain the average flux. The space charge density, ρ_e, is related to the potential (ϕ) by the Poisson equation (equation (S10))

$$\nabla \cdot (\varepsilon_R \nabla \phi) = -\frac{\rho_e}{\varepsilon_0} \tag{S10}$$

where ε_R is the relative permittivity of the electrolyte solution, ε_0 is the permittivity of free space, and ρ_e is the space charge density is given by

$$\rho_e = F \sum_{i=1}^{m} z_i c_i \tag{S11}$$

The Poisson equation combined with mass transport:

$$\frac{\partial c_i}{\partial t} = -\nabla \cdot \overrightarrow{N_i} = 0 \tag{S12}$$

allows determination of the flux of species i given by the Nernst-Planck equations:

$$\overrightarrow{N_i} = -D_i \nabla c_i - \mu_i z_i c_i \nabla \phi + c_i \vec{u} \tag{S13}$$

Here, D_i is the coefficient of diffusion, ∇c_i is the concentration gradient, μ_i is the ionic mobility, z_i is the valence, c_i is the concentration of each species i in the nanochannel, $\nabla \phi$ is the electric field, and $\vec{u}$ is the velocity of the fluid flow. The ionic mobility is given by Einstein's relation, $\mu_i = D_i F/RT$, where R is the universal gas constant, and T is the absolute temperature.

The inlet microchannel reservoir potential was set to 5 V while the outlet microchannel potential was set to 4.999 V. This gives an electric field of 2kV/m in the numerical model to match the experimental case V_a = 5V by using scaling methodology we have reported previously.[S23] Details of the nanochannels being operated under both V_a = 3V and V_a = 5V have been reported previously[S1] and the 5V case was chosen here as a representative example. The continuity equation and the steady-state Navier-Stokes equations for an incompressible fluid were used for the velocity (equations (S14) and (S15)).

$$-\nabla p + \eta \nabla^2 \vec{u} - \rho_e \nabla \phi = 0 \quad \text{(S14)}$$

$$\nabla \cdot \vec{u} = 0 \quad \text{(S15)}$$

where η is the fluid viscosity and ∇p is the pressure gradient.

The size of the reservoirs was selected to ensure that the potential was constant in the reservoirs and that effects of the reservoir surface charge were minimal i.e., cation and anion concentration is equal to bulk concentration in the reservoir, except near the charged walls.[S24] The walls were impermeable to flow with a no slip boundary condition for the velocity. The concentration in the reservoirs was set to the bulk electrolyte concentration, which was 1 mM for KCl and 0.33 mM for $CaCl_2$. The concentration of H^+ in the reservoir was set to 10^{-pH} and the concentration of OH^- to $10^{-(14-pH)}$. A constant surface charge boundary condition was used for the potential at each of the charged walls according to[S24]

$$\sigma = -\varepsilon_e \frac{d\phi}{dy}$$

$$\sigma = -\varepsilon_e \frac{d\phi}{dx} \quad \text{(S16)}$$

Here, σ is the surface charge density, ε_e is the permittivity of the electrolyte, and ϕ is the potential in the channel. The predicted conductance was obtained by dividing the calculated current by the applied axial potential. The magnitude of the surface charge density, σ, was used as a fit parameter to match the simulated conductance with the experimentally measured conductance.

A second case was numerically compared for both electrolytes as a function of pH to determine if there is any significant effect due to possible heterogeneous surface charge density between the glass and PDMS walls as discussed in the main manuscript. The values of the surface charge density input into COMSOL Multiphysics for both cases for 1 mM KCl and 0.33 mM $CaCl_2$ are listed in Table S3 and Table S4 respectively. In Case 1, $\sigma_{PDMS} = \sigma_{glass}$. In Case 2, $4\sigma_{PDMS} = \sigma_{glass}$, however, the total surface charge ($wL\sigma_{PDMS} + wL\sigma_{glass}$) was fixed between the two cases. A similar model with heterogeneous surface

charge density was performed for $CaCl_2$. The values of the surface charge density are listed in Table S3 for 1 mM KCl and Table S4 for 0.33 mM $CaCl_2$.

Table S3. Values of the surface charge density as a function of pH used in COMSOL simulations for 1 mM KCl. The total surface charge ($wL\sigma_{PDMS} + wL\sigma_{glass}$) remains fixed for both cases.

KCl	**Case 1: Homogenous Surface Charge** $\sigma_{PDMS} = \sigma_{glass}$			**Case 2: Heterogeneous Surface Charge** $4\sigma_{PDMS} = \sigma_{glass}$		
pH	Surface Charge Density (C/m^2) Glass	Surface Charge Density (C/m^2) PDMS	Total surface charge ($wL\sigma_{PDMS} + wL\sigma_{glass}$) (pC)	Surface Charge Density (C/m^2) Glass	Surface Charge Density (C/m^2) PDMS	Total surface charge ($wL\sigma_{PDMS} + wL\sigma_{glass}$) (pC)
2	0	0	0	0	0	0
4	0	0	0	0	0	0
6	-0.0017	-0.0017	-0.085	-0.0027	-0.0007	-0.085
7	-0.0025	-0.0025	-0.125	-0.0040	-0.0010	-0.125
8	-0.0042	-0.0042	-0.210	-0.0067	-0.0017	-0.210
10	-0.0045	-0.0045	-0.225	-0.0072	-0.0018	-0.225

Table S4. Values of the surface charge density as a function of pH used in COMSOL simulations for 0.33 mM $CaCl_2$. The total surface charge ($wL\sigma_{PDMS} + wL\sigma_{glass}$) remains fixed for both cases.

$CaCl_2$	**Case 1: Homogenous** $\sigma_{PDMS} = \sigma_{glass}$			**Case 2: Heterogeneous Surface Charge** $4\sigma_{PDMS} = \sigma_{glass}$		
pH	Surface Charge Density (C/m^2) Glass	Surface Charge Density (C/m^2) PDMS	Total surface charge ($wL\sigma_{PDMS} + wL\sigma_{glass}$) (pC)	Surface Charge Density (C/m^2) Glass	Surface Charge Density (C/m^2) PDMS	Total surface charge ($wL\sigma_{PDMS} + wL\sigma_{glass}$) (pC)
2	0	0	0	0	0	0
4	0	0	0	0	0	0
6	0	0	0	0	0	0
7	-0.0010	-0.0010	-0.050	-0.0016	-0.0004	-0.050
8	-0.0017	-0.0017	-0.085	-0.0027	-0.0007	-0.085
10	-0.0016	-0.0016	-0.080	-0.0026	-0.0006	-0.080

The intrinsic conductance for all four cases (2 each for KCl and $CaCl_2$) calculated using COMSOL Multiphysics are shown in Figure S4 with further discussion in the main manuscript. Numerical solutions were verified for mesh independence with a relative tolerance for convergence set to 10^{-6}. The numerically computed conductances for the homogenous and heterogeneous surface charge distribution cases differed

by less than 2% for both KCl and $CaCl_2$ showing that the intrinsic conductance is independent of likely unequal surface charge density on the top and bottom walls. The intrinsic conductance, therefore, is determined by the total surface charge on the walls and the resulting space charge in the nanochannel volume as a function of pH. As expected, the intrinsic conductance was dominated by electromigration (93% total current), followed by convective flux contributing ~7%. Contribution of diffusive flux towards the overall current was negligible.

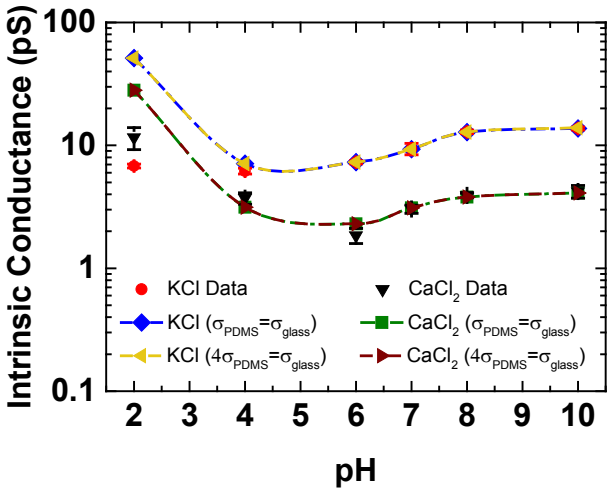

Figure S4. Numerically computed and experimentally measured intrinsic nanochannel conductance as a function of pH. The numerically computed conductances for the homogenous and heterogeneous surface charge distribution cases differed by less than 2% for both KCl and $CaCl_2$. The dashed lines are intended as eye-guides.

ESTIMATION OF BARE SURFACE CHARGE DENSITY AND INTERACTION PARAMETER

As noted in the main manuscript, interactions between multivalent counter ions (i.e., those with opposite polarity to the wall charge) in the electrolyte with the charged wall and/or with each other are known to cause charge inversion at sufficiently high electrolyte concentration. While there is no consensus in the literature about the mechanism by which charge inversion occurs for divalent ions, the concentration where charge inversion is expected ranges from 10 mM for strongly correlated liquid theory based on ion-ion interactions [S3,16] to 350 mM or higher based on other previous reports.[S25-27] The pH data for 0.33 mM $CaCl_2$ and the observed transition for conductance of divalent electrolytes and mixtures in the main

manuscript occur at concentrations below 10 mM, the lowest reported concentration for charge inversion for divalent cations. However, for completeness the interaction parameter was calculated to ensure ion-ion interactions do not significantly affect the system reported here.

The interaction parameter depends on the value of the bare or native surface charge density. The bare surface charge density (σ_{bare}) is given by the sum of the contributions from each type of ionizable surface group,[S28-30]

$$\sigma_{bare} = e(\Gamma^{+} - \Gamma^{-}) \tag{S17}$$

where Γ^{+} is the total number of positively charged surface sites, Γ^{-} is the total number of negatively charged surface sites, and e is the elementary charge. For silica, negative surface sites arise from the deprotonation of surface silanol groups according to the reaction,[S28-30]

$$SiOH \rightleftharpoons SiO^{-} + H^{+} \tag{S18}$$

where, the equilibrium constant, pK_1 for the deprotonation reaction can be written from the law of mass action as [S28,31]

$$\frac{[H^{+}]_S \Gamma^{SiO^{-}}}{\Gamma^{SiOH}} = 10^{-pK_1}\ (Mol/l) \tag{S19}$$

Here pK_1 determines the equilibrium number of ionized surface groups as a function of pH. The surface proton concentration ($[H^{+}]_S$) was assumed to follow a Boltzmann distribution[S28-31]

$$[H^{+}]_S = [H^{+}]_B \exp\left(-F\phi_S/_{RT}\right) \tag{S20}$$

Where, the bulk proton concentration ($[H^{+}]_B$) is related to the solution pH by

$$[H^{+}]_B = 10^{-pH}\ \left(\frac{Mol}{l}\right) \tag{S21}$$

Subsequently, the equation for the surface charge density is given by

$$\sigma = \frac{-e\Gamma\left(10^{-pK_1+pH}\exp\left({}^{F\phi_S}/_{RT}\right)\right)}{1+10^{-pK_1+pH}\exp\left({}^{F\phi_S}/_{RT}\right)} \quad \text{(S22)}$$

An independent solution for the surface charge density as a function of surface potential was also obtained by implementing the Poisson-Boltzmann description of the ion distribution near the charged wall.[S28-30] Given the ULAR nanochannels (here, aspect ratio = 0.0005)[S32] with near-infinite length (2.5 mm) with respect to 16 nm channel depth, the Poisson equation was written in a 1-D form with a Boltzmann distribution for the space charge density, and solved analytically for σ. The equation for the surface charge density for a symmetric monovalent electrolyte is,

$$\sigma = \sqrt{8RT\varepsilon_e I_S}\,sinh\left(\frac{zF}{2RT}\zeta\right) \quad \text{(S23)}$$

which is the well-known Grahame equation for a monovalent symmetric electrolyte. The zeta potential (ζ) is related to the surface potential (ϕ_S) by[S31]

$$\phi_S = \frac{\sigma_S + C_{Stern}\zeta}{C_{Stern}} \quad \text{(S24)}$$

where, the Stern layer capacitance, C_{Stern} was 2.9 F/m^2 [S29-31]. Equations (S22) and (S23) were solved self-consistently for σ and ζ for a 1:1 electrolyte as a function of pH. Here the ionic strength, I_s is given by

$$I_S = \frac{1}{2}\sum {z_i}^2 c_i \quad \text{(S25)}$$

For estimation of the bare surface charge density, a single pK value was used for both the glass and PDMS surfaces. As discussed above the intrinsic conductance captures the average surface charge density. Further, a previous report[S33] showed that glass and PDMS have similar pK values and thus similar change in surface charge density as a function of pH. Figure S5 shows the well-known profile for the bare surface charge density as a function of pH plotted alongside the average surface charge density results from COMSOL Multiphysics (main manuscript). A pK_1 value of 7.5 best fits or even overestimates the

monovalent electrolyte surface charge density in the pH range where no ion-surface interactions for K^+ are expected.

For strongly correlated liquid theory to apply $\Gamma \gg 1$ where Γ is the interaction parameter given by

$$\Gamma = \frac{\sqrt{\sigma_{bare} z^3 e^3/\pi}}{4 k_b T \varepsilon_R \varepsilon_0}$$

Here σ_{bare} is the bare surface charge density, z is the ion valence, e is the elementary charge, $k_b T$ is the thermal energy and ε_R and ε_0 are the relative and vacuum permittivity. The interaction parameter at pH 7 for divalent cations is $\Gamma = 0.66$, corresponding to weak ion-ion correlations[S26,34,35] therefore, ion-ion interactions are neglected. The reduction in surface charge density for divalent cations is, therefore, attributed to ion-surface interactions.

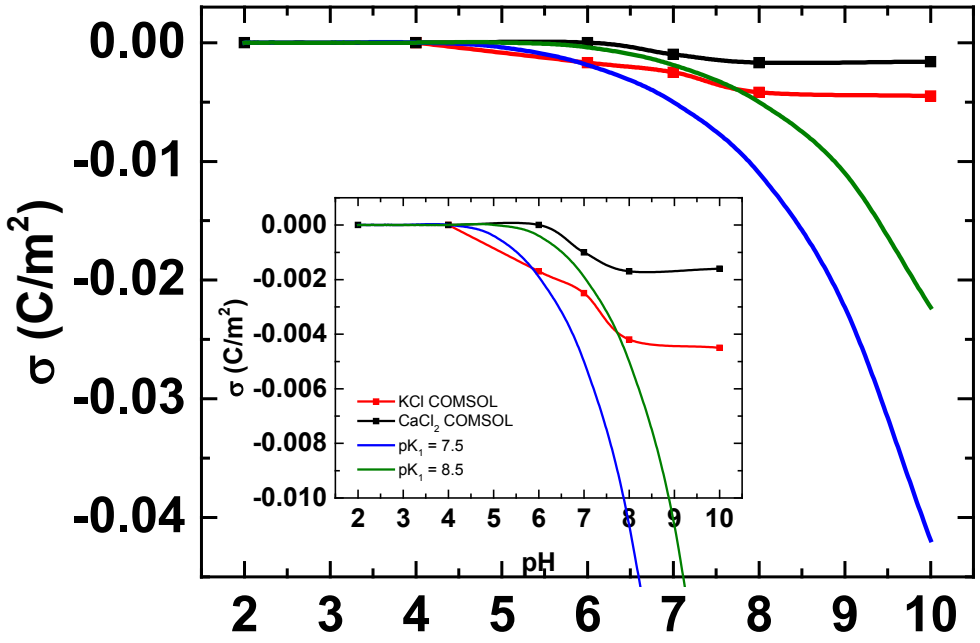

Figure S5. The surface charge density calculated via COMSOL compared to an estimation for the bare surface charge density (above). The inset shows a zoomed in view.

SUPPORTING INFORMATION REFERENCES

(S1) Fuest, M.; Boone, C.; Rangharajan, K. K.; Conlisk, A. T.; Prakash, S. *Nano Letters* **2015**, *15*, 2365–2371.

(S2) Ai, Y.; Liu, J.; Zhang, B.; Qian, S. *Sensors and Actuators B: Chemical* **2011**, *157*, 742-751.

(S3) Guan, W.; Fan, R.; Reed, M. A. *Nature Communications* **2011**, *2*, 506.

(S4) Liu, Y.; Huber, D. E.; Tabard-Cossa, V.; Dutton, R. W. *Applied Physics Letters* **2010**, *97*, 143109.
(S5) Karnik, R.; Fan, R.; Yue, M.; Li, D.; Yang, P.; Majumdar, A. *Nano letters* **2005**, *5*, 943-948.
(S6) Fan, R.; Huh, S.; Yan, R.; Arnold, J.; Yang, P. *Nature Materials* **2008**, *7*, 303-307.
(S7) Nam, S. W.; Rooks, M. J.; Kim, K. B.; Rossnagel, S. M. *Nano letters* **2009**, *9*, 2044-2048.
(S8) Singh, K. P.; Kumari, K.; Kumar, M. *Journal of Applied Physics* **2011**, *110*, 084301.
(S9) Yusko, E. C.; An, R.; Mayer, M. *ACS Nano* **2010**, *4*, 477-487.
(S10) Rutkowska, A.; Edel, J. B.; Albrecht, T. *ACS Nano* **2013**, *7*, 547-555.
(S11) Joshi, P.; Smolyanitsky, A.; Petrossian, L.; Goryll, M.; Saraniti, M.; Thornton, T. J. *Journal of Applied Physics* **2010**, *107*, 054701.
(S12) Horiuchi, K.; Dutta, P. *Lab on a Chip* **2006**, *6*, 714-723.
(S13) Shin, S.; Kim, B. S.; Song, J.; Lee, H.; Cho, H. H. *Lab on a Chip* **2012**, *12*, 2568-2574.
(S14) Oh, Y. J.; Bottenus, D.; Ivory, C. F.; Han, S. M. *Lab on a Chip* **2009**, *9*, 1609-1617.
(S15) Schoch, R. B.; Renaud, P. *Applied Physics Letters* **2005**, *86*, 253111.
(S16) Li, S. X.; Guan, W.; Weiner, B.; Reed, M. A. *Nano Letters* **2015**, *15*, 5046–5051.
(S17) Duan, C.; Majumdar, A. *Nature Nanotechnology* **2010**, *5*, 848-852.
(S18) Stein, D.; Kruithof, M.; Dekker, C. *Physical Review Letters* **2004**, *93*, 035901.
(S19) Martins, D. C.; Chu, V.; Conde, J. P. *Biomicrofluidics* **2013**, *7*, 034111.
(S20) Conlisk, A. T. *Essentials of Micro- and Nanofluidics*, 1st ed.; Cambridge University Press: New York, 2013, p 552.
(S21) Prakash, S.; Yeom, J. *Nanofluidics and Microfluidics: Systems and Applications*; William Andrew: Norwich, NY, 2014.
(S22) Nishizawa, M.; Menon, V.; Martin, C. *Science* **1995**, *268*, 700-702.
(S23) Rangharajan, K. K.; Fuest, M.; Conlisk, A. T.; Prakash, S. *Microfluidics and Nanofluidics* **2016**, *20*, 54.
(S24) Jin, X.; Aluru, N. R. *Microfluidics and Nanofluidics* **2011**, *11*, 297–306.
(S25) Lorenz, C. D.; Travesset, A. *Physical Review E* **2007**, *75*, 061202.
(S26) van der Heyden, F. H. J.; Stein, D.; Besteman, K.; Lemay, S. G.; Dekker, C. *Physical Review Letters* **2006**, *96*, 224502.
(S27) He, Y.; Gillespie, D.; Boda, D.; Vlassiouk, I.; Eisenberg, R. S.; Siwy, Z. S. *Journal of the American Chemical Society* **2009**, *131*, 5194-5202.
(S28) Datta, S.; Conlisk, A. T.; Li, H. F.; Yoda, M. *Mechanics Research Communications* **2009**, *36*, 65-74.
(S29) Jiang, Z.; Stein, D. *Physical Review E*, **2011**, *83*, 031203.
(S30) Jiang, Z.; Stein, D. *Langmuir* **2010**, *26*, 8161–8173.
(S31) Behrens, S. H.; Grier, D. G. *Journal of Chemical Physics* **2001**, *115*, 6716-6721.
(S32) Pinti, M.; Kambham, T.; Wang, B.; Prakash, S. *Journal of Nanotechnology in Engineering and Medicine* **2013**, *4*, 020905.
(S33) Kirby, B. J.; Hasselbrink, E. F. *Electrophoresis* **2004**, *25*, 187-202.
(S34) Faraudo, J.; Travesset, A. *The Journal of Physical Chemistry C* **2007**, *111*, 987-994.
(S35) Shklovskii, B. I. *Physical Review E* **1999**, *60*, 5802-5811.